Biomimetic mineralization of diatom exoskeleton for sustainable pH-sensitive colored chitosan/silica hybrid self-supported films

Sandra Castanié, Laurent Billon

Materials & Design 250 (2025) 113571

Contents lists available at ScienceDirect

Materials & Design

journal homepage: www.elsevier.com/locate/matdes

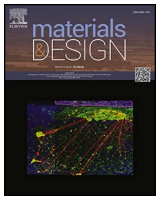

Biomimetic mineralization of diatom exoskeleton for sustainable pH-sensitive colored chitosan/silica hybrid self-supported films

Sandra Castanié [a,b], Laurent Billon [a,b,*]

[a] Bio-Inspired Materials Group: Functionalities & Self-Assembly, E2S UPPA, 64000 Pau, France
[b] Université de Pau et Pays de l'Adour, E2S UPPA, CNRS, IPREM UMR 5254, Institut des sciences analytiques et de physico-chimie pour l'environnement et les matériaux, 64000 Pau, France

ARTICLE INFO

Keywords:
Hybrid films
Chitosan/silica
Bio-inspired material
Diatoms
pH sensor
Alizarin organic dye

ABSTRACT

A gentle bio-inspired approach to the biosilicification occurring in diatom frustule is proposed to develop, at room temperature and without addition of a co-solvent, self-supported hybrid organic/inorganic films with pH-sensitive properties. It was found that chitosan (CS) biopolymer, a polysaccharide possessing numerous amine groups ($–NH_2$) is capable of mimicking the action of the silaffins proteins of diatom frustule in the polycondensation process of the TetraEthoxyOrthoSilicate (TEOS) silica precursor to form a cohesive self-supported hybrid film under soft conditions in aqueous media. Thanks to its good film-forming property, hybrid chitosan/silica (CS/SiO_2) films have been elaborated varying the amount of TEOS to study their optical and mechanical properties. It is shown that increasing the amount of TEOS up to 90 wt% improves the transparency, strength and stability of the films due to the interpenetration of the chitosan and silicaq networks. The incorporation of sustainable pH-sensitive alizarin dye during the elaboration of the films does not affect their mechanical properties whatever the composition. Moreover, these colored hybrid materials show good pH-sensitiveness under basic environment. Therefore, thanks to their antimicrobial properties and their pH-sensitivity, such self-supported films could be designed for applications such as smart sustainable food packaging and food degradation indicator.

1. Introduction

Biomimicry, or bio-inspiration, which involves observing Nature and copying it or part of it to develop human concepts, technologies and designs, is an approach that has already led to the development of high-performance technologies, and that finds numerous applications in fields such as physics and chemistry [1–6], energy [7,8], medicine [9–12], architecture and design [13], and robotics [14,15].

Taking inspiration from Nature to adopt a biomimicry approach is also an exciting challenge to aim to a more sustainable world. Natural materials can exhibit remarkable properties made of relatively weak constituents due to performant hierarchical structures and hybridation between inorganic and organic constituents. In marine organisms, wonderful performing materials are obtained through very soft conditions of temperature, concentration, or pressure. For instance, nacre from mollusks shells exhibits a remarkable strength and toughness while composed of greater than 95 % aragonite, a brittle ceramic, but incorporating 5 % of soft biopolymer into a hierarchical structure. Nacre from Abalone shells is ~1000 times tougher than pure aragonite [16,17]. Diatoms are also great examples of inspiring materials due to their original shell structure. Made of transparent amorphous silica, the frustule, *i.e.* the shell, presents a hierarchized double porosity, mainly micrometric but with nanometric pores at the bottom of the micropores, which insures protection to living cell while allowing nutrients and UV to enter for feeding and photosynthesizing [18]. The process of biosilicification leading to the specific frustule structure involves organic parts for the polycondensation at room temperature of silica dissolved in water. This polycondensation is driven by the complexation of silicic acid $Si(OH)_4$ by amine groups $–NH_2$ present in great number in proteins called silaffins, to form the diatom cell based on an organic/inorganic hybrid material [19–21].

With the view to get inspiration from these natural and soft processes to develop performing materials, to resort to biopolymers and organic/inorganic hybridation appears to be a good and sustainable strategy

* Corresponding author at: At Bio-Inspired Materials Group: Functonalities & Self-Assembly, Université de Pau et Pays de l'Adour, E2S UPPA, CNRS, IPREM UMR 5254, Institut des sciences analytiques et de physico-chimie pour l'environnement et les matériaux, 64000 Pau, France.
E-mail address: laurent.billon@univ-pau.fr (L. Billon).

https://doi.org/10.1016/j.matdes.2024.113571
Received 11 September 2024; Received in revised form 17 December 2024; Accepted 25 December 2024
Available online 28 December 2024

followed by an important scientific community [22–25]. In the particular case of the biosilicification process occurring in diatom frustules, the biopolymer candidate must have numerous amine groups –NH_2 able to mimic the action of silaffins in the polycondensation of silica precursor into a silica film [21]. Among biodegradable polymers, chitosan (CS) is a linear polysaccharide composed of randomly distributed β-(1 → 4)-linked *D*-glucosamine (deacetylated unit) and *N*-acetyl-*D*-glucosamine (acetylated unit). With its protonated amine functions at slightly acidic pH, it appears to be of interest to mimic the silica complexation process of diatom. Moreover, chitosan presents the advantages to be one of the most abundant natural food sources, to be biocompatible and nontoxic, to be a good film-forming, to resist to the soft heat and to have a good adsorption capacity. These properties permit to find a lot of applications in various fields such as medicine, cosmetics, photography, depollution, or food packaging [26]. However, the poor solubility of chitosan limits its application and processing convenience.

Chitosan/silica (CS/SiO_2) hybrids have recently received much attention due to improvement in chemical and mechanical properties of chitosan thanks to the addition of silica nano-particles [27–30]. Moreover, the introduction of silica into biomaterials can increase its oxygen permeability, biocompatibility and biodegradability [31].

The sol–gel process is a well-known technique in soft chemistry permitting to combine organic and inorganic parts to develop materials with attractive properties. Here, considering the good film-forming property of chitosan, the sol–gel route can be an effective way to develop interpenetrated chitosan/silica hybrid films with enhanced chemical and physical properties.

If some papers describe the formation of CS/SiO_2 hybrid films, these last ones are elaborated by simple mixing of silica nano-particles with chitosan, or requiring temperature or co-solvent [32–34]. Nevertheless, to mimic the soft conditions and the chemical reaction which takes place during the process of biosilicification of diatoms, the process has to occur in aqueous media under soft conditions. A such bio-inspired approach was recently described by Larrieu *et al.* [35] to form CS/SiO_2 films that mimic the composition of the diatom frustule.

Moreover, due to the soft conditions, the sol–gel process was also described to permit the incorporation of additives such as pigments and dyes. Colorimetric pH indicators are of great interest in many fields of science due to their easy production in a wide range of colors and a broad range of applications [36,37]. Synthetic dyes such as bromothymol blue, bromocresol green, cresol red or methyl red are commonly used in the industry of pH-sensitive indicators [37–40]. However, they present an important risk for health and environment due to their toxicity, carcinogenicity and poor degradability [41]. In the last decade, renewable materials have attracted more and more attention and efforts are underway to replace toxic synthetic chemicals with natural or sustainable compounds. As coloring agents, natural dyes have been used for thousands of years but they present the disadvantages to be instable and to rapidly degrade and fade under temperature and light [42]. However, the last years have seen an important investment of scientists in the development of stabilized organic dyes within inorganic supports. The inorganic matrix offers high thermal stability, mechanical strength and solvent resistance, while the organic component provides coloring and functionality [42,43]. Among the natural organic dyes, anthocyanins and anthraquinone pigments are of interest for their pH-sensitiveness. These class of molecules are commonly obtained from fruits and plants such as blueberries, sweet potatoes, red cabbage, madder [44]. Alizarin (1,2-dihydroxy-9,10-anthracenedione, AZ) is considered as one of the most popular and stable dyes due to its high resistance to light degradation. It has been widely used in the painting and fabric industry [45], in dye-sensitized solar cells [46], as marker of calcium biochemical assays [47], or as an indicator to monitor food quality [48,49].

Herein, we propose to highlight the bio-inspired and sustainable approach mimicking the biosilicification occurring in the diatom frustule to design pH-sensitive self-supported and flexible chitosan/silica/dye hybrid films via a simple sol–gel aqueous route in soft conditions. The incorporation of bio-sourced alizarin and of various silica contents in their composition was considered. Chemical/structural characterization, optical/film-forming properties and pH-sensitiveness of the films were investigated.

This approach in aqueous media under soft conditions represents a sustainable route to develop cohesive self-supported hybrid silica films with designed properties based on chitosan and *in-situ* generation of silica.

2. Materials and methods

2.1. Raw materials

Chitosan powder (DDA ≈ 82 %, Mw = 50–150 kDa) was purchased from GTC Bio. Tetraethyl orthosilicate (TEOS, 99 %) and anhydrous magnesium sulfate ($MgSO_4$) powder were purchased from ABCR. Acetic acid (99 %), hydrochloric acid (37 %), dehydrated calcium chloride ($CaCl_2$), sodium chloride (NaCl), potassium chloride (KCl) and alizarin dye (AZ) were purchased from Sigma-Aldrich. Magnesium chloride hexahydrated and potassium hydroxide (KOH) were purchased from Merck. Buffers were purchased from Carl Roth. Scheme 1 presents the chemical formula of chitosan, TEOS and alizarin.

2.2. Hybrid films preparation

2.2.1. Chitosan/silica hybrid films

Chitosan/silica hybrid films were prepared in soft conditions using sol–gel route with TEOS as source of silica. As chitosan is soluble in acid water, CS powder was dissolved in a 2 wt% acetic acid solution (2 g of acetic acid for 98 g of MilliQ water), to obtain a 4 wt% solution, and was stirred at room temperature for 48 h until complete dissolution. The pH of the CS precursor solution was measured by pH-meter equal to 4.3 at 21 °C. TEOS was diluted in MilliQ water to obtain a 4 wt% solution. The pH of the TEOS precursor solution was measured by pH-paper equal to about 5.

The two precursor solutions were then mixed together varying the amount of TEOS from 0 wt% to 90 wt%. The different mixtures were stirred for 30 min at room temperature and the pH of the solutions was evaluated by pH-paper. Then the solutions were casted onto polycarbonate plates, or glass or quartz microscope slides and placed under fume hood to dry out. After 24 h, dried cohesive films of 10–150 μm were obtained.

2.2.2. Chitosan/silica/alizarin hybrid films

pH-sensitive CS/SiO_2 hybrid films containing alizarin dye were synthesized following the same procedure. Films were obtained by adding AZ powder at a concentration of $4x10^{-4}$ M with the different CS/TEOS mixtures. AZ concentration was chosen in accordance with the poor solubility of the dye in acid media. Before stirring for 30 min, the mixtures were placed 5 min into ultrasounds to avoid alizarin aggregates. The solutions were then deposited onto polycarbonate plates, or glass or quartz microscope slides and placed under fume hood to dry out.

2.3. Characterization methods

2.3.1. Fourier-transform infrared (FTIR) spectroscopy

The structure of the hybrid films was examined by Fourier-transform infrared (FTIR) spectroscopy (Model Thermo Fisher Nicolet IS50). The spectra were recorded in attenuated total reflectance (ATR) mode and the wavelength range was between 4000 and 500 cm^{-1}. For the analysis self-supported films were prepared.

2.3.2. Solid-state nuclear magnetic resonance spectroscopy

^{13}C and ^{29}Si solid state nuclear magnetic resonance (NMR) spectra were recorded on a Bruker AVANCE III 500WB spectrometer. Prior to the measurements, the films were cryo-grinded to obtain flakes of

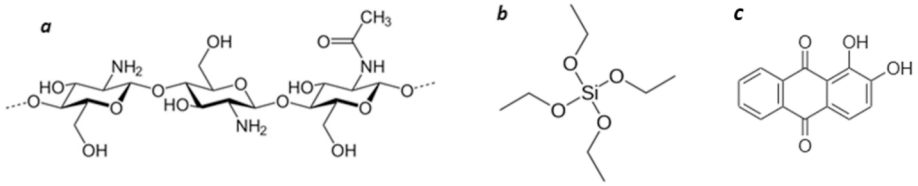

Scheme 1. Chemical formula of a) partially deacetylated chitosan, b) TEOS and c) alizarin.

maximum 0.5 mm in width. ^{13}C spectra were recorded with a 4 mm triple X/Y/Z probe using the CP MAS technique and the adamantane reference (28 ppm). The number of scans performed was 2200, with a recycle delay of 7 s and a contact time of 2 ms. ^{29}Si spectra were recorded with a 4 mm double H/X probe using the HPDEC technique and the octakis(trimethylsiloxy)silsesquioxane (Q8M8) reference at 12.4 ppm. The number of scans performed was 500, with a recycle delay of 150 s.

2.3.3. Scanning electron microscopy + Energy dispersive spectroscopy (SEM-EDS)

SEM images of the films' surfaces were recorded on a MEB-FEG Apreo 2 $^{@TFS}$ using an accelerated voltage of 2 kV. All samples were sputtered with 4 nm of platinum before analyses using a high-resolution sputter coater Cressington 208HR. Chemical analysis was recorded using a Bruker EDS XFlash 6I100 at an accelerated voltage of 5 kV.

2.3.4. Atomic force microscopy (AFM)

AFM adhesion images were recorded using a Bruker AFM Multi-Mode8® on PeakForce QNM mode (ScanAsyst-Air probe), at 2 kHz. For these analyses the films were deposited on a silicon wafer.

2.3.5. Mechanical properties of films

Mechanical properties of hybrid CS/SiO_2 films with and without AZ were determined at room temperature using a universal materials tester Alliance RT/50 (Material Testing Systems) equipped with pneumatic jaw. Measurements were performed with a 50 Hz acquisition speed and a 20 mm/min speed test. Previous to the tests, all samples were dried under extractor hood at room temperature during 2 days and stored in petri boxes. The sample thickness was measured at least 3 times randomly using an electronic digital micrometer with a resolution of 0.0001 mm. For the thickest sample (100 % chitosan) the variation of thickness did not exceed 0.036 mm. For the thinnest (90 wt% TEOS), the variation did not exceed 0.001 mm. Between the different compositions, the thicknesses varied from 0.01 for the samples with 90 wt% TEOS to 0.121 mm for pure chitosan films. All the films were cut into rectangular shapes (80 x 10 mm) to test the tensile strength (TS; MPa) and the elongation at break (EAB; %). TS and EAB were calculated using Eq. (1) and Eq. (2), respectively. A minimum of five specimens were tested for each composition. The results given are the average and deviation of the different tests made for a same composition.

$$TS(MPa) = F_{max}/S \quad (1)$$

where F_{max} is the maximum load, and S is the cross-sectional area of the film.

$$EAB(\%) = (L - L_0)/L_0 \times 100 \quad (2)$$

where L is the length at which the film breaks, and L_0 is the initial length of the sample.

2.3.6. Stability into water solutions and water uptake

The stability of the CS/SiO_2 and CS/SiO_2/AZ hybrid films was studied into two different solvents. MilliQ water (pH = 6.4) was used in comparison with an artificial sea water prepared according to the Roscoff station protocol. Composition is given in the Supporting Information **Table S1**. The samples were immersed into aqueous media for 48 h to appreciate their stability. Water uptake tests were performed on films oven dried at 40 °C for a night and weighed (W1). The samples were then immersed in MilliQ water (test 1) and in artificial sea water (test 2) at room temperature for 1 h to reach the equilibrium. Excess water was removed with filter paper from the swollen saturated films, which were subsequently weighed for the determination of wet weight (W2). The samples were then put back into water for 1 h to repeat the test. 7 measurements were performed. Water uptake (W) of the hybrids was obtained according to the following equation:

$$W(\%) = \frac{w_2 - w_1}{w_1} \times 100\% \quad (3)$$

2.3.7. Contact angle measurements

The apparent contact angle measurement was realized with an optical device (GBX contact angle meter, DGD Fast/60) which allow to determine the contact angle of a droplet with the surface. A drop of MilliQ water or artificial sea water was deposited on a sol–gel coated glass microscope slide. Final values are the average of 4 replicates obtained at different spots.

2.3.8. Optical properties of alizarin and hybrid films

The optical properties of the materials were studied by UV–visible spectroscopy on a Shimadzu UV-21021PC spectrometer. Transmittance spectra (300–800 nm) were recorded on CS/SiO_2 hybrid films to evaluate the effect of SiO_2 ratio on the transparency of the films. Absorbance spectra (300–800 nm) of AZ solutions and AZ-containing hybrid films were performed to characterized their pH-sensitivity.

2.3.9. Az-containing hybrid films pH-sensing experiment

The pH-sensitivity of the hybrid films containing AZ was evaluated by UV–visible spectroscopy either after exposure to acid and basic atmospheres, or by deposition of acid and basic drops to mimic liquid projections. The films were elaborated onto quartz microscopy slides to avoid deformation in contact with the liquid.

For the tests under atmosphere, the films were either first exposed to an acid atmosphere created by a solution of HCl at pH 5 for 24 h. Then, the same films were exposed to a basic atmosphere for another 24 h (KOH pH 12). Or, they were first exposed to a basic atmosphere (buffer pH 10) for 6 h, then to an acid atmosphere (buffer pH 3) for 24 h. To create the desired atmosphere, the solution was place in small caps and put together with the films in a close petri box. Previously to the experiment, the UV–vis spectrum of each films was registered as reference. Then, after each step, the corresponding UV–vis spectrum was recorded.

For the tests by deposition of acid and basic drops, we proceeded first by the exposure to the acid solution (HCl pH 5). After 1 min, the excess of liquid was removed with a filter paper and the UV–vis spectrum was recorded. Then, multiple drops of a basic solution (KOH pH 10) were deposited on the surface of the film to "wash" the traces of acid before recording the next spectrum. The procedure was repeated a second time and finished with the deposition of acid drops (**Table S2**).

3. Results and discussion

3.1. Nature of interaction between silica and chitosan networks

As preliminary verification of the interaction capacity between silica and chitosan networks, the pH of the precursor solutions and the mixtures were compared with the Point of Zero Charge point of silica (PZC = 2). At 21 °C, the pH of the chitosan precursor solution (4 wt% in acid acetic solution) is equal to 4.3 (pH-meter measurement). Comparatively, the pH of all the mixture solutions were determined to be in the same acid range (pH paper comparison), meaning that the pH of the solutions is always higher than silica PZC. In that conditions, silica particles are negatively charged due to predominance of $Si\text{-}O^-$ groups, which gives them a hydrophilic character favorable to electrostatically interact with the NH_3^+ groups of chitosan.

3.2. Chemical structure of the films

The structure of the hybrid films was first studied by FTIR-ATR spectroscopy to evaluate the influence of the CS:TEOS ratio onto the network structure. Fig. 1 shows comparison between pure CS film and CS/SiO_2 with 90 wt% TEOS. Spectra of all other compositions are given in the Supporting Information (**Fig. S1**).

For pure chitosan film spectrum, bands associated with the vibration of primary amines bonds ($–NH_2$) around 1404 cm^{-1} and secondary amines bonds (–NH-) around 1538 cm^{-1} are present, as well as the residual amide absorption band around 1645 cm^{-1} attributed to the incomplete deacetylation of chitosan. Other bands characteristic of C–H stretching mode of chitosan are also visible between ≈ 900–1100 cm^{-1} and around 2877 cm^{-1}. Then, for all compositions incorporating TEOS, the characteristic bands of chitosan remain visible. For comparison, all the spectra were normalized on the C–H bond of chitosan at 2877 cm^{-1}. The incorporation of TEOS in the composition of the films is marked by the appearance of new bands around 1022 and 786 cm^{-1} attributed to the vibration of siloxane bonds (respectively Si-O-Si asymmetric and symmetric stretching mode [50,51]), and around 950 cm^{-1} associated with Si-OH. The presence of these signals shows that the hydrolysis of TEOS and the condensation of silica successfully occurred in these soft conditions of reaction. Moreover, a band around 1052 cm^{-1} could be associated with Si-O-C symmetric stretching vibrations [52]. According to Bravo-Flores *et al.*[53] and Liu *et al.*[54], the existence of this band would confirm that chitosan intervenes in the condensation of Si-OH to form the Si-O-C bonds, limiting the self-condensation between Si-OH. At this stage, the FTIR signals are not enough clear to assume with evidence the presence of a covalent bond between the two networks because the frequency signal is located in the region of the strong band of the Si-O-Si asymmetric vibration, but also because this band could indicate that the hydrolysis of TEOS is incomplete.

Also, while in the literature the peak around 786 cm^{-1} is mostly attributed to the symmetric stretching mode vibration of silica, Ohishi *et al.* [55] and Larrieu *et al.* [35] have associated this band with Si-N vibration indicating a creation of a link between Si and N, *i.e.* a covalent bond between the silica and the chitosan, creating then a cross-linked networks.

Similar results are observed for the whole TEOS compositions (**Fig. S1**). By increasing TEOS amount, the band characteristic of the Si-O-Si bonds vibrations (around 1062 cm^{-1} and 1019 cm^{-1}), and of the potential Si-O-C bond around 1062 cm^{-1} are more and more intense, as well as the peak observed at 786 cm^{-1}. Conversely, the bands around 1404 cm^{-1} and 1538 cm^{-1} which are characteristic of the amine groups, are less and less intense while TEOS replaced chitosan in the composition.

The same analyses were performed on the films incorporating AZ dye to determine the impact of the pigment introduction during the reaction process on the final structure of the films. The CS/SiO_2 and CS/SiO_2/AZ films spectra with 90 wt% of TEOS are compared in Fig. 2**A** and Fig. 2**B**. For both compositions, the characteristic peaks of primary amines bonds ($–NH_2$) around 1404 cm^{-1} and secondary amines bonds (–NH-) around 1538 cm^{-1} of chitosan, the silica (Si-O-Si) vibrations (around 1022 cm^{-1}), and the peak at around 1052 cm^{-1} that could correspond to a Si-O-C bond are observed, meaning that the introduction of alizarin in the composition of the hybrid films is not affecting the formation of the networks. As in the case of the films without alizarin, amine characteristic peaks are less intense in the film with 90 wt.%TEOS than for pure CS/SiO_2 film, due to the diminution of chitosan in the composition. Similar observations are obtained for the different CS:TEOS ratio confirming the network formation (**Fig. S2A**).

Fig. 2**C** gives the alizarin raw powder spectrum (black line) and shows the comparison between a pure chitosan film and films with 90 wt % TEOS with and without alizarin.

Among the characteristic bands of anthraquinone molecules, alizarin spectrum shows a broad band around 3400 cm^{-1} characteristic of the hydroxy group OH. The band at 1662 cm^{-1} is characteristic of the C=O carbonyl groups, and the bands at 1586 and 1450 cm^{-1} correspond to the C=C of the aromatic rings, both of the anthraquinone molecules. First, it is worth noting that the characteristic peaks of alizarin are not observed on the different films containing the dye. This is probably due to the weak amount of pigment into the films (4.10^{-4} wt%) that are overlapped with the other bands from chitosan and silica. In the case of the films containing 90 wt% TEOS with and without alizarin, the slight intensity differences in the range of 1200–500 cm^{-1} are probably due to inhomogeneities of composition. These differences are observed for all the films containing 60 wt% TEOS and more (**Fig. S2C**).

Solid NMR spectroscopy was used in addition to ATR-FTIR to

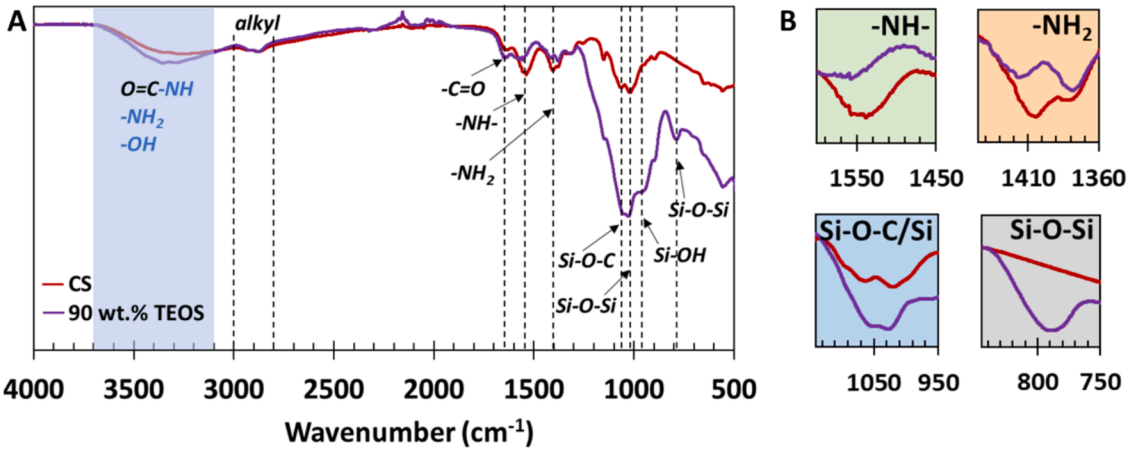

Fig. 1. A) ATR-FTIR spectra of CS/SiO_2 hybrid films with 0 wt% and 90 wt% of TEOS. B) Zoom on –NH-, $–NH_2$, Si-O-C and Si-O-Si specific bands.

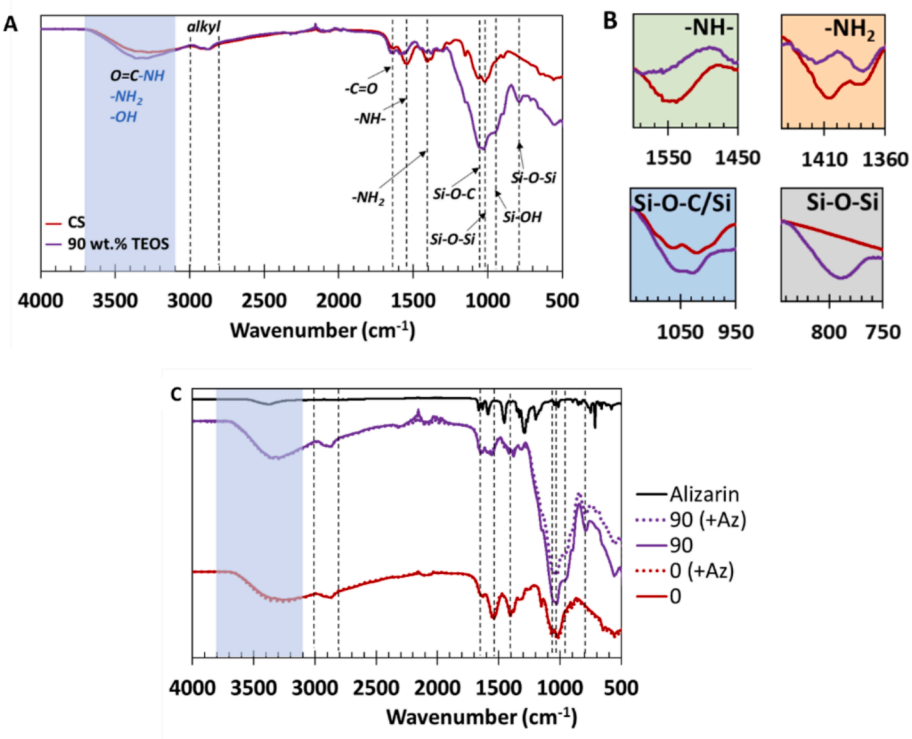

Fig. 2. ATR-FTIR spectra of A) CS/SiO_2 /AZ hybrid films with 0 wt% and 90 wt% of TEOS, B) Zoom on –NH-, –NH_2 , Si-O-C and Si-O-Si specific bands, and C) comparison between CS/SiO_2 hybrid films and CS/SiO_2 /AZ hybrid films with 0 wt% and 90 wt% of TEOS.

investigate the formation of bonds between the chitosan and silica networks and/or with alizarin. Fig. 3**A** shows the ^{13}C and ^{29}Si NMR spectra of alizarin dye and CS/SiO_2 films containing 0, 50 and 90 wt% of TEOS without and with alizarin.

Whatever the composition of the films, similar spectra are obtained. The peaks observed are characteristic of chitosan with around 173 ppm a peak that corresponds to the –NH**CO**CH_3 function in correlation with the peaks between 25 and 102 ppm, characteristic of a saccharide moiety. The peak centered at 180 ppm is then attributed to the **–COOH** function of the residual acetic acid used as solvent for the solubilization of the chitosan. The similarity of the spectra of chitosan film without and with TEOS indicates the non-specific interaction/reaction between the two networks *via* Si-C bond. Concerning alizarin, after 15 h of accumulation, no aromatic signal characteristic of the dye or new chemical bond were detected on the films due to its weak concentration.

The ^{29}Si NMR spectra of the same films (Fig. 3**B**) show an important dilution of the silica network into the films, but the signals demonstrate the presence of Q sites around −110 (Q_4), −100 (Q_3) and −91 ppm (Q_2) in similar proportions whatever the composition of the films (**Fig. S3** and **Table S3**), indicating the presence of Si-O-C bonds and so confirming the observation of the Si-O-C FTIR band that could correspond to a covalent bonding between the two networks or the incomplete hydrolysis of TEOS. Nevertheless, no specific T sites peaks are observed around −80 (T_3), −70 (T_2) and −62 ppm (T_1) which could indicate the creation of Si-N or Si-C bonds between the chitosan and silica networks.

Thus, according to FTIR and NMR analyses, the structure of the CS/SiO_2 and CS/SiO_2/AZ films obtained by sol–gel route in soft conditions can be described either as semi-interpenetrated chitosan and silica networks linked by electrostatic interactions, or as interpenetrated networks if linked through Si-O-C covalent bonds as shown in Scheme 2**.**

Films homogeneity. SEM/EDS (Fig. 4) analyses were performed on the surfaces of pure CS and CS/SiO_2 films containing 50 and 90 wt% of TEOS to study their structuration and homogeneity while increasing TEOS amount. On SEM images (Fig. 4**a–c**), the films' surfaces appeared similarly homogeneous with a small rugosity that seems to be slightly smoother for the film containing 90 wt% of TEOS. The homogeneity of

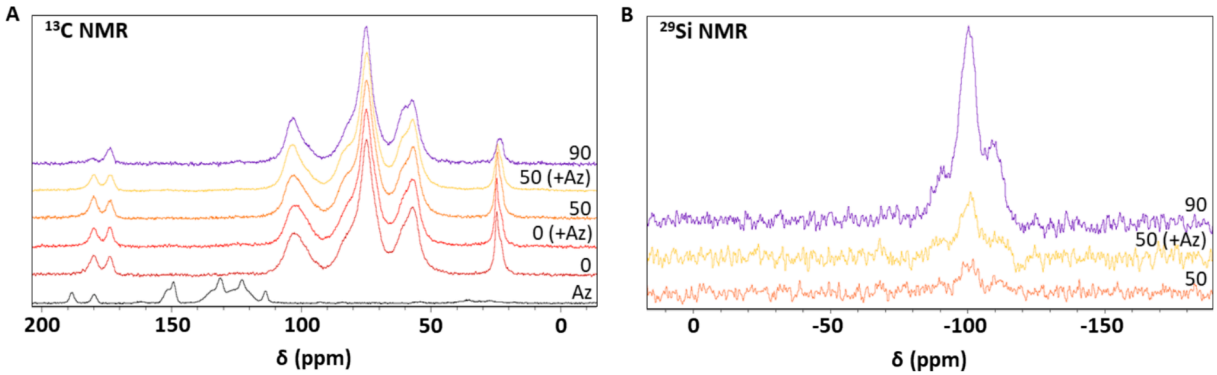

Fig. 3. A) Solid state ^{13} C NMR spectra of alizarin and CS/SiO_2 films containing 0, 50 and 90 wt% of TEOS; B) Solid state ^{29} Si NMR spectra of CS/SiO_2 films containing 50 and 90 wt% of TEOS.

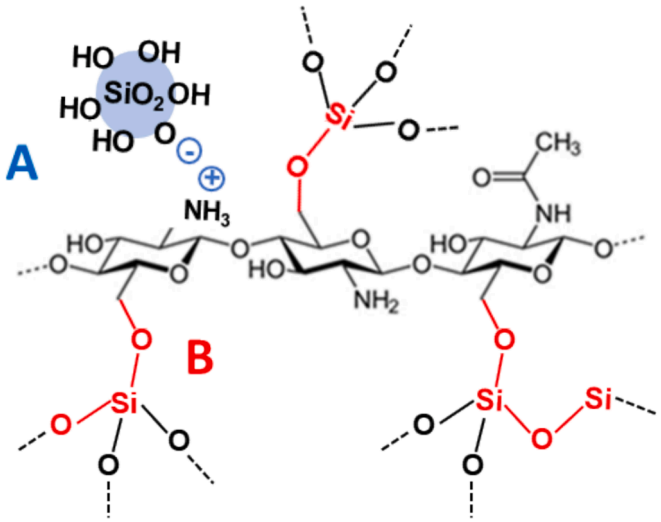

Scheme 2. Schematic representation of the interactions between chitosan and silica networks through A) electrostatic interactions between silica nanoparticles and chitosan, and B) covalent Si-O-C bonds.

the films was confirmed by EDS chemical analyses. Indeed, spectra on Fig. 4**d–f** give evidence of the growing presence of silicon while increasing the amount of TEOS in the films, and Fig. 4**g** and Fig. 4**h** show their good dispersion/distribution through silicon mapping.

The films surfaces were also analyzed on AFM in adhesion mode (**Fig. S4**). Images show again a good homogeneity of the films without significant differences depending on their composition. No evidence of nano or microdomains was observed by AFM or SEM.

3.3. Mechanical properties of films

The CS/SiO_2 hybrid films without and with AZ were studied through tensile tests. Fig. 5 shows photos of 100 % CS testing samples and CS/SiO_2 hybrid containing 90 wt% of TEOS. Photos of the testing samples of all other compositions are given in **Fig. S5**. The Young modulus (YM), the tensile strength (TS) and the elongation at break (EAB) parameters are reported in Fig. 6**A**, Fig. 6**B**, and Fig. 6**C** respectively. The tensile stress *versus* strain curves are given in **Fig. S6**.

It is worth noting that the films prepared with pure CS had a Young modulus around 1 450 MPa (Fig. 6**A**). The addition of TEOS in the composition of the hybrid films significantly increases the YM to reach about 4 000 MPa for the films containing 80 and 90 wt% TEOS. The tensile strength tends also to increase by addition of TEOS. Pure CS films show a TS of 46 MPa, while films with 80 and 90 wt% TEOS have a TS of 68 and 55 MPa, respectively, representing 48 and 20 % of improvement. The weaker TS observed for 60 and 90 wt% TEOS might be due to inhomogeneities in the CS/SiO_2 networks.

The increase in YM and TS of CS-based films incorporating silica is in accordance within the literature [56,57], showing that the soft

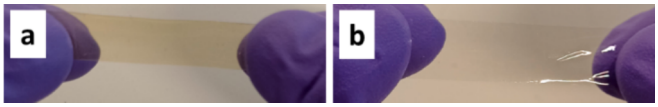

Fig. 5. Photos of a) 100% CS testing samples and b) CS/SiO_2 hybrid containing 90 wt% of TEOS.

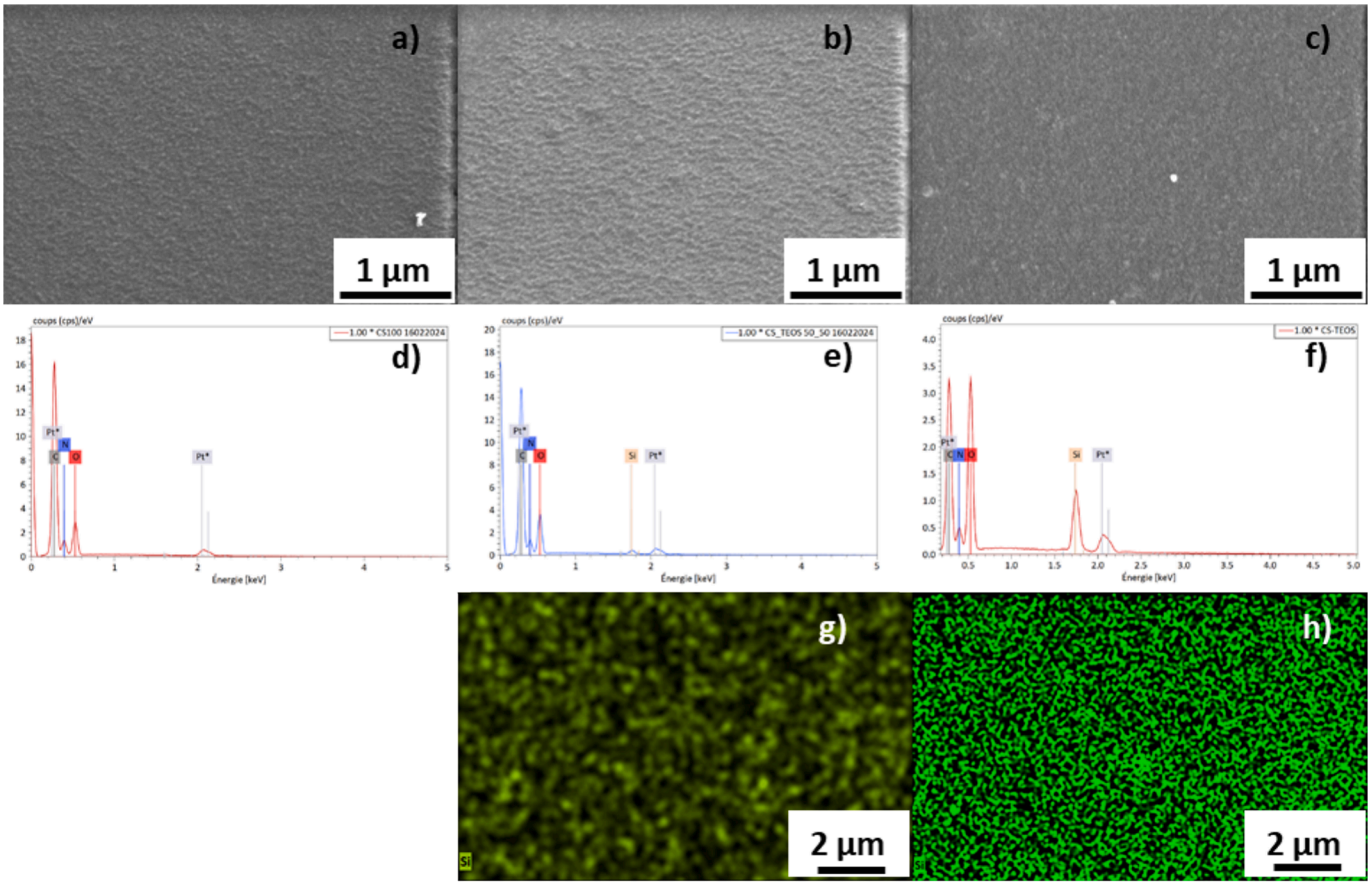

Fig. 4. SEM/EDS analyses of pure CS film surface (a, d), CS/SiO_2 containing 50 wt% of TEOS (b, e, g), and 90 wt% of TEOS (c, f, h). a), b) and c) are the SEM images. d), e) and f) are the EDS spectra. g) and h) correspond to the silicon EDS map.

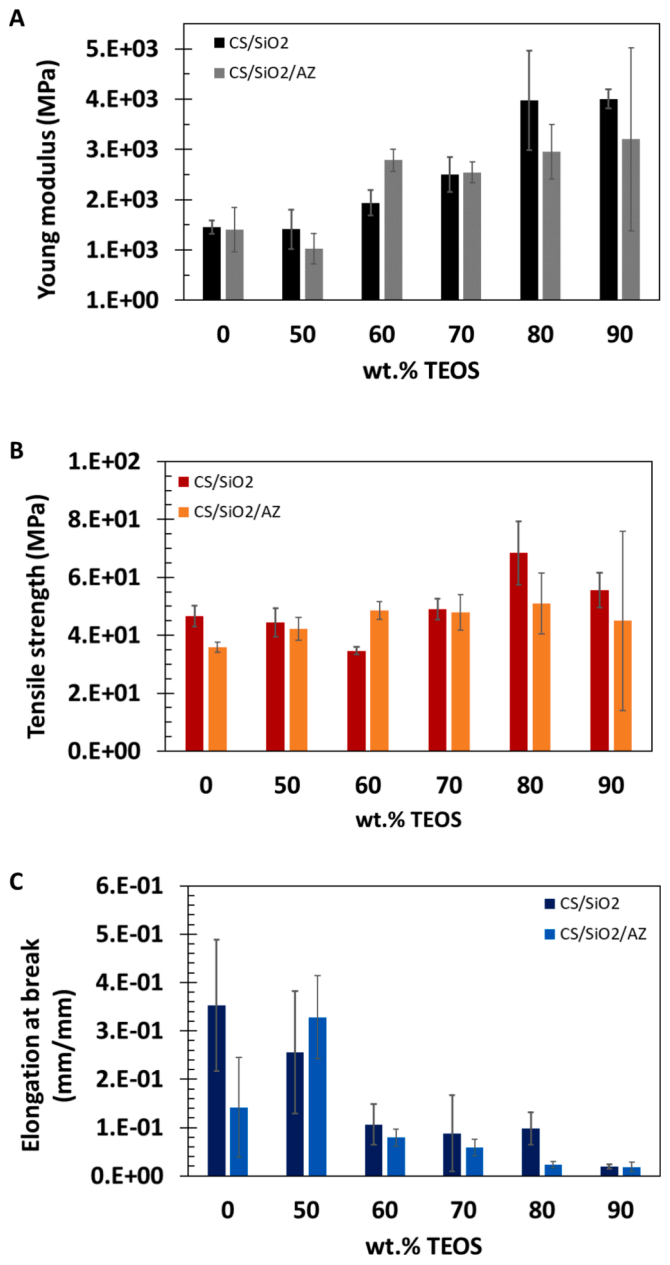

Fig. 6. A) Young Modulus, B) Tensile strength and C) Elongation at break of CS/SiO_2 and CS/SiO_2 /AZ hybrid films with 0 wt%, 50 wt%, 60 wt%, 70 wt%, 80 wt% and 90 wt% of TEOS.

conditions used herein allow to create films with higher strength with a large extend of compositions.

Conversely, it is observed that the substitution of CS by TEOS significantly reduces EAB (Fig. 6**C**) from 35 mm/mm for pure CS films to 2 mm/mm for 10/90 wt% CS/TEOS films.

The increase in stiffness and tensile strength resistance by addition of silica into the films compositions, while decreasing their ductility, is attributed to the interpenetration of the chitosan and silica networks as shown by FTIR and ^{29}Si NMR analyses, and to the formation of hydrogen/electrostatic interactions [58]. Therefore, the amount of TEOS incorporated into the films will have to be adjusted in accordance with the targeted applications to reach the corresponding strength to flexibility balance.

Similar mechanical properties of hybrid films containing alizarin are observed. At this low concentration of dye, no significant differences are observed between the films without and with AZ. Slightly weaker mechanical properties could be observed, nevertheless it can be considered in margin of error (less than 5 %). Young modulus increases from 1 406 MPa for CS/AZ to 3 202 MPa for CS/SiO_2/AZ films containing 90 wt% TEOS, representing an improvement of 128 %. An improvement of 42 % of the tensile strength is obtained by the substitution of chitosan with 80 wt% of TEOS for CS/SiO_2/AZ films. Finally, elongation at break measurements show a reduction from 33 mm/mm for CS/SiO_2/AZ films containing 50 wt% TEOS to 2 mm/mm for CS/SiO_2/AZ films containing 90 wt% TEOS.

If the addition of TEOS seems to drastically change the mechanical properties of the hybrid films, the presence of a very small amount of AZ does not impact the final properties of the colored hybrid films.

3.4. Films stability into aqueous media and swelling ratio

Stability and swelling tests were performed by immersing the films in MilliQ water (pH = 6.4) and in artificial sea water (pH = 8.2). These two different media were chosen to evaluate the influence of pH/salts on the solubility of the films. After 1 h of immersion in MilliQ water, pure chitosan films and films containing up to 60 wt% TEOS were dissolved while all others compositions (70 wt%, 80 wt% and 90 wt% TEOS, without and with alizarin) stayed stable until the end of the test (48 h). In artificial sea water, all the films stayed stable until the end of the test. These results show evidence that chitosan network is affected by the acid conditions. Amino groups of CS could be protonated in acid conditions leading to positively charge groups $–NH^{3+}$. Electrostatic repulsion between these groups is then responsible for the network swelling until its dissolution [59]. It appeared also that the substitution of chitosan by more than 60 wt% of TEOS helped to prevent dissolution of the films in acid conditions by increasing the semi-interpenetration of the silica network with the macromolecular chains. This phenomenon could be also in accordance with the presence of covalent bonds between chitosan and silica networks that could increase through the addition of TEOS.

Swelling properties of the CS/SiO_2 hybrid films without and with alizarin were studied to measure the hydration of the chitosan/silica network. Fig. 7 shows swelling ratio (SR) measured in MilliQ water (Fig. 7**A**) and in artificial sea water (Fig. 7**B**), after 1 h of immersion in the media to reach the equilibrium.

In both conditions, SR depends on the TEOS content in the composition of the films. In MilliQ water, the SR ratio could not be measured for films containing less than 60 wt% TEOS due to their dissolution. For the other compositions, increasing the proportion of TEOS reduces the SR from about 500 % up to 50 % for films with 70 and 90 wt% TEOS, respectively (Fig. 7**A**). In artificial sea water (pH = 8.2), a maximum SR of about 155 % is observed for pure chitosan films and up to 50 wt% TEOS in the composition (Fig. 7**B**). It then decreases with the augmentation of TEOS ratio to stabilized around 70 to 50 % for films containing more than 80 wt% of TEOS. Liu *et al.* [60] had reported that the swelling properties of chitosan based films containing nanosilica spheres were decreased with the increase of nanosilica. Indeed, as chitosan films form a dense network with dispersed nanosilica, it decreases the number of hydrophilic groups. They also reported the same tendency for the pH effect on the swelling properties of CS/SiO_2 hybrid films. They observed that the swelling ratio of their films at pH 2.6 was rather higher than films at pH 7.6 whatever the amount of silica [60].

In both conditions of pH, results were similar for films containing alizarin dye meaning that this last one does not affect the cohesion of the films at this low concentration.

3.5. Wettability measurement

Contact angle measurements were performed both with MilliQ water and artificial sea water to minimize the influence of the pH on the results due to water absorption. Fig. 8**A** presents values obtained after deposition of MilliQ water drops on the surface of the films without and with

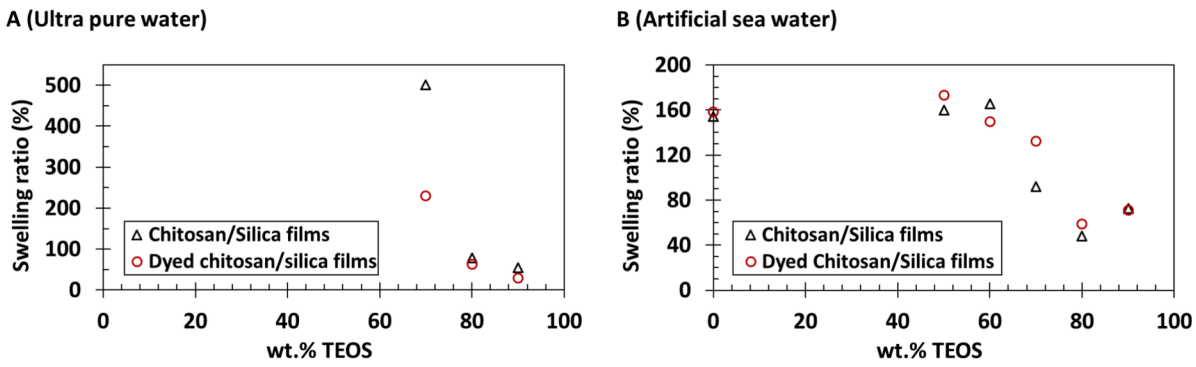

Fig. 7. Swelling ratio of CS/SiO_2 and CS/SiO_2 /AZ hybrid films with 0 wt%, 50 wt%, 60 wt%, 70 wt%, 80 wt% and 90 wt% of TEOS. In MilliQ water (A) and artificial sea water (B).

alizarin.

Results are similar in both cases meaning that the presence of alizarin does not modify the wettability of the films. Pure chitosan films show a contact angle of 76° and 78° without and with alizarin respectively. Hydrophily of the film surfaces seems to slightly decrease while increasing the amount of silica, to reach 83° for the films containing 70 wt% TEOS. Above 70 wt% TEOS, the contact angle decreases to equal the value of pure chitosan films. The same tendency was observed for the tests with artificial water (Fig. 8**B**). This could be due to a competition between the wettability of the films and a fast diffusion of the water drop into the film.

Even though we expected to obtain the reinforcement of hydrophily of the films due to the augmentation of silica in the composition, the difference in contact angle values was not significant. That could be explained by the presence of chitosan at the surface of the hybrid films whatever their composition [35].

3.6. Optical properties of the films

The optical properties of the hybrid films were measured both in transmittance and in absorbance spectroscopy in the range of 250–800 nm. The films were deposited onto glass plates to obtain a flat surface. Fig. 9**A** gives a comparison in transmittance between CS and CS/SiO_2 hybrid films containing 90 wt% TEOS, with and without alizarin. Spectra of all the other compositions are given in the Supporting Information (**Fig. S7**). Fig. 9**B** shows the corresponding absorbance spectra. Relative values could not be compared due to differences in the films' thicknesses (**Table S4**).

Nevertheless, it was observed that the different films present a good transparency to visible light between 800 and 500 nm. At smaller wavelengths, chitosan films present an important absorbance, particularly around 310 nm. This loss in transparency is much less pronounced for the film with 90 wt% TEOS, and is attributed to the decrease in chitosan amount for this composition. For the films containing alizarin, no significant differences are observed in the spectra except in the region 500–550 nm where a slight broad absorbance peak is visible and attributed to the orangish color of the pigment.

3.7. pH-sensitiveness of CS/SiO_2/AZ hybrid films

An interesting property of alizarin dye is its important pH sensitiveness resulting in a wide range of colors. This can be advantageous for abnormal acid or basic conditions detection for food packaging, by example. The influence of the pH conditions on the chemical structure and the color of alizarin is presented in Fig. 10.

At pH lower than 5.2, AZ is fully protonated and the solution appears to be orange-yellow with a UV absorption spectrum centered at 460 nm. Between pH 8 and pH 10, AZ solutions are observed to be orange-red. This protonation/deprotonation process is reversible in this range of pH. The absorption peak at 460 nm is shifted to 515–530 nm and a second absorption peak is observed at 330 nm. The hydroxyl group in β position is deprotonated. At pH higher than 10, the second hydroxyl group, *i.e.* in α position, is then also deprotonated leading to a purple solution. The absorption spectra show peaks at 530 nm, 568 nm and 608 nm. The peak at 330 nm tends to be shifted to wavelengths lower than 300 nm while pH value increases.

The pH-sensitiveness of AZ into films was evaluated by UV–vis spectroscopy both under acid/basic atmospheres (Fig. 11) and by drop deposition of an acid/basic solutions (Fig. 12).

Fig. 11 shows the results obtained on CS/AZ and CS/SiO_2/AZ (90 wt % TEOS) films, either exposed first to an acid atmosphere (Fig. 11**A,B**) or first to a basic atmosphere (Fig. 11**C,D**). For the test performed first under acid conditions, it can be seen a clear change in color from orange to purple after 24 h under basic atmosphere (pictures on Fig. 11**A,B**). These results indicate that alizarin is sensitive to its environment while incorporated into the films. This pH-sensitiveness is also visible on the

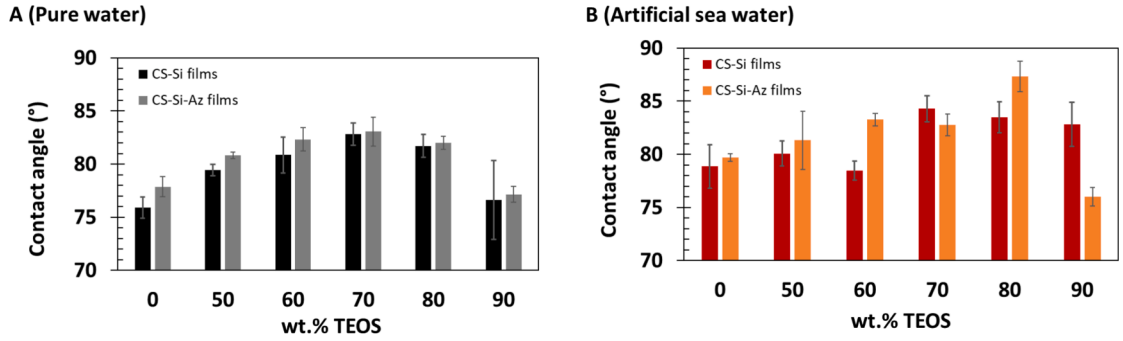

Fig. 8. Contact angle measurements for CS/SiO_2 and CS/SiO_2 /AZ hybrid films with 0 wt%, 50 wt%, 60 wt%, 70 wt%, 80 wt% and 90 wt% of TEOS. A) Using MilliQ water, and B) using artificial sea water.

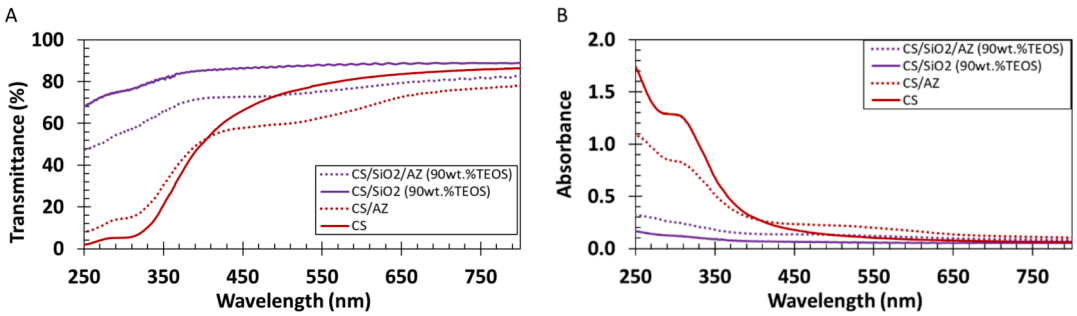

Fig. 9. UV-light spectra of CS and CS/SiO_2 hybrid films with 90 wt% of TEOS with and without alizarin in A) transmittance, and B) absorbance mode.

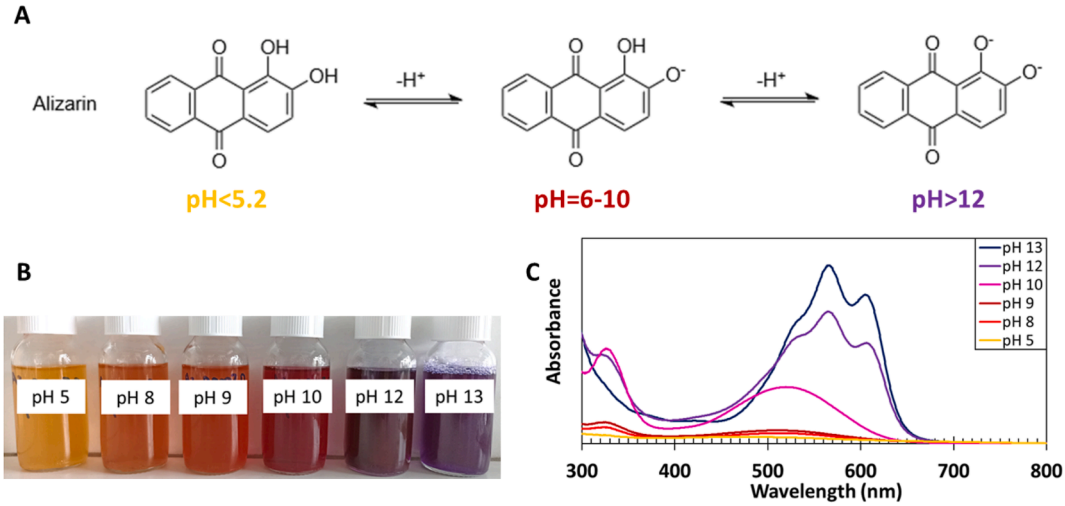

Fig. 10. A) Chemical forms of alizarin dye at different pH, B) Photos of alizarin at different pH in buffer solutions (2.10^{-4} M) and C) UV–vis spectra of alizarin in buffer solutions at different pH.

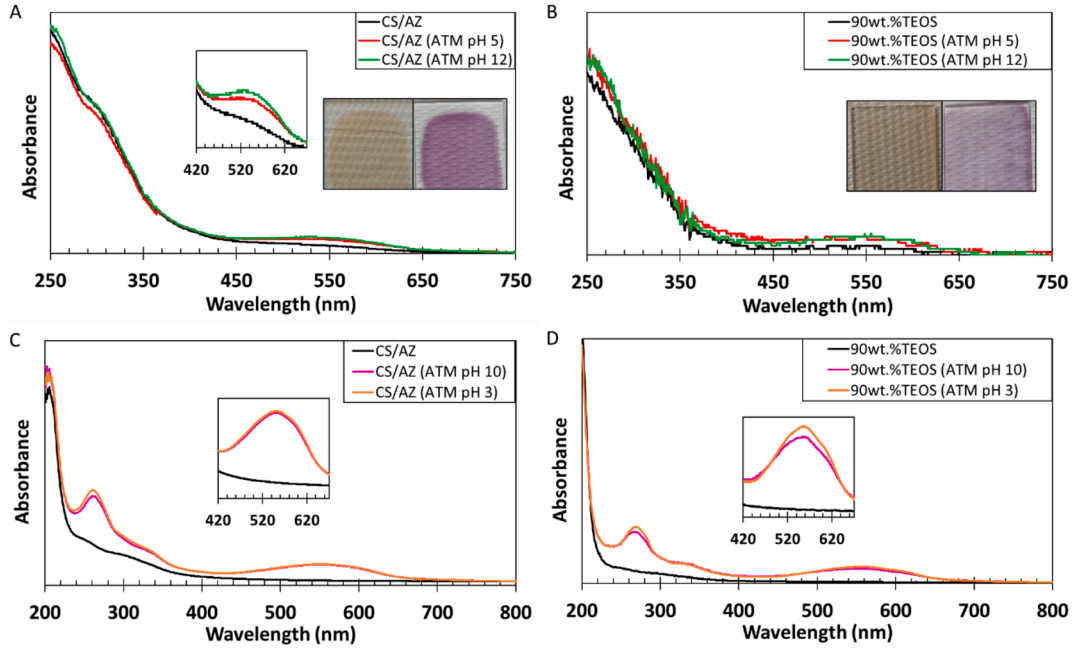

Fig. 11. UV–vis spectra in absorbance of A, C) CS/AZ films and B, D) CS/SiO_2 /AZ films containing 90 wt% TEOS, under acid and basic atmosphere. Figures A, B) refer to the test first performed under acid then basic atmosphere. C and D) refer to the test first performed under basic then acid atmosphere.

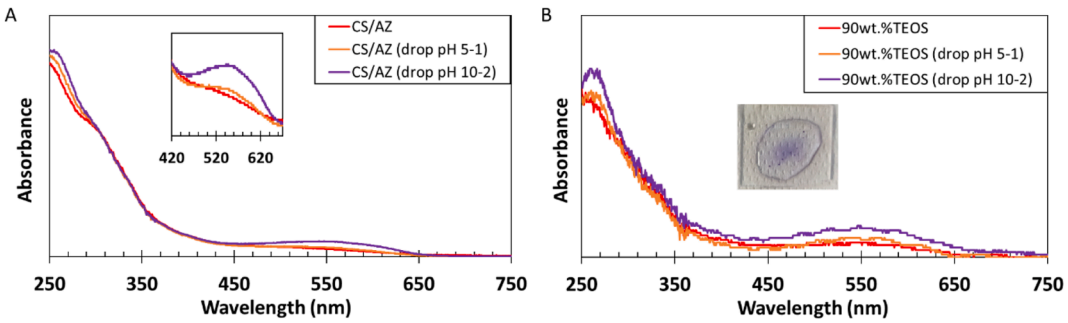

Fig. 12. UV–vis spectra in absorbance of A) CS/SiO_2 films and B) CS/SiO_2 /AZ films with 90 wt% TEOS, under acid and basic projections.

UV–vis spectra with a slight increase of the bands around 250 nm, 300 nm and 550 nm. This behavior goes in favor of an increase of the pH around AZ as presented previously (Fig. 10). Moreover, it also seems to indicate that in the reference films, alizarin is in an acid environment lower than pH 5 which correspond to the synthetic conditions (chitosan powder was solubilized in a 2 wt% acid acetic solution). Similar results were obtained for the other composition tested (CS/SiO_2/AZ with 70wt.%TEOS). When the films are first exposed to a basic environment (Fig. 11**C,D**), the spectra showed again an increase in the intensity of the characteristic bands at 250 nm, 300 nm and 550 nm and the films become purple. Nevertheless, no reversibility of the pH-sensing was observed. Similar results were obtained for all other compositions tested (CS/SiO_2/AZ with 50wt.%TEOS and CS/SiO_2/AZ with 70wt.%TEOS) (**Fig. S8**).

The reversibility of the pH-sensing of CS/SiO_2/AZ films was then studied by successive depositions of acid and basic drops on the films surface. First, some HCl solution drops @ pH 5 were deposited on the samples surface and the corresponding spectra were register after 1 min of exposure (sample drop pH 5–1). Then, multiple KOH solution drops @ pH 10 were deposited on the same area (enough to wash the acid solution used before) and the corresponding spectrum was registered (sample drop pH 10–2). Results are presented on Fig. 12**A** and Fig. 12**B**, *i.e.* respectively CS/AZ and CS/SiO_2/AZ 90wt.%TEOS films.

Similar behaviors are observed for the tests 1 and 2, respectively under acid then basic conditions compared to previous acid/basic atmospheres (Fig. 11**A,B**). Indeed, an intensity increase of the characteristic bands is visible associated with a bathochromic effect, *i.e.* slight shift to the higher wavelengths. Analogous results are obtained for the other films compositions (**Fig. S9**). Nevertheless, due to the films swelling, we observed a pigment desorption/release (see insert Fig. 12**B**) decreasing drastically the dye content and making reversibility tests non-significant (tests 3, 4 and 5, respectively acid pH 5, basic pH 12, acid pH5). Here in a more sustainable approach, it is worth noting that the alizarin dye can be chemically modified to be grafted on macromolecules [61] to avoid leaching and so a one-shot pH-sensor. Nevertheless, this last point can be turned in a positive way to develop one-shot pH-sensitive film for food protection to avoid fraud or reconditioning.

4. Conclusion

Mimicking the biosilicification occurring in the diatom frustule to obtain hybrid organic/inorganic films was possible using a sustainable approach with chitosan biopolymer to polycondense *in-situ* silica from tetraethoxysilane (TEOS) precursor *via* a simple sol–gel aqueous route in soft conditions. We showed that:

(1) self-supported cohesive hybrid silica films can be obtained varying the TEOS amount from 0 to 90 wt%;
(2) it was possible to design the mechanical and optical properties of the films managing the TEOS content. Nevertheless, as chitosan is soluble into acid media, a minimum amount of 70 wt% of TEOS was necessary to keep a cohesive film in MilliQ water while the films are stable in saline solution mimicking Atlantic Ocean water.
(3) it is possible to incorporate a pH-sensitive organic dye without affecting the films properties.
(4) at this stage, the use of alizarin showed that the dye is still sensitive to its environmental conditions while incorporated in the films whatever the composition.

If only one-shot reversibility of the pH-sensitiveness of the colored films was demonstrated due to the release of the dye, for future improvements, alizarin dye could be grafted to develop sustainable pH-sensing films [61–63] for multiple uses as food packaging to follow the expiry date or food degradation, especially.

CRediT authorship contribution statement

Sandra Castanié: Writing – review & editing, Writing – original draft, Investigation, Formal analysis, Data curation. **Laurent Billon:** Writing – review & editing, Validation, Supervision, Resources, Project administration, Methodology, Investigation, Funding acquisition, Formal analysis, Conceptualization.

Declaration of competing interest

The authors declare the following financial interests/personal relationships which may be considered as potential competing interests: [Laurent Billon reports financial support was provided by Rectorat de Bordeaux. If there are other authors, they declare that they have no known competing financial interests or personal relationships that could have appeared to influence the work reported in this paper].

Acknowledgment

The authors thank E2S UPPA and Rectorat Nouvelle Aquitaine for the financial support of the “DSG2 Biomimétisme” project, and the S.C. fellowship especially.

Appendix A. Supplementary material

Supplementary data to this article can be found online at https://doi.org/10.1016/j.matdes.2024.113571.

Data availability

No data was used for the research described in the article.

References

[1] G.D. Bixler, B. Bhushan, Rice and butterfly wing effect inspired low drag and antifouling surfaces: a review, Crit. Rev. Solid State Mater. Sci. 40 (2015) 1–37, https://doi.org/10.1080/10408436.2014.917368.

[2] Y. Li, J. Krahn, C. Menon, Bioinspired dry adhesive materials and their application in robotics: a review, J. Bionic. Eng. 13 (2016) 181–199, https://doi.org/10.1016/S1672-6529(16)60293-7.
[3] X. Gao, Z. Guo, Biomimetic superhydrophobic surfaces with transition metals and their oxides: a review, J. Bionic Eng. 14 (2017) 401–439, https://doi.org/10.1016/S1672-6529(16)60408-0.
[4] P. Marcasuzaa, H. Yin, Y. Feng, L. Billon, CO $_2$ -Driven reversible wettability in a reactive hierarchically patterned bio-inspired honeycomb film, Polym. Chem. 10 (2019) 3751–3757, https://doi.org/10.1039/C9PY00488B.
[5] P. Marcasuzaa, M. Save, P. Gérard, L. Billon, When a pH-triggered nanopatterned shape transition drives the wettability of a hierarchically self-organized film: a bio-inspired effect of "sea Anemone,, J. Colloid Interf. Sci. 581 (2021) 96–101, https://doi.org/10.1016/j.jcis.2020.07.130.
[6] H. Xue, F. Liu, Z. Wang, D. Liu, L. Zhou, W. Su, S. Niu, Z. Han, L. Ren, Bio-inspired dual-responsive photonic crystal with smart responsive hydrogel for pH and temperature detection, Mater. Des. 233 (2023) 112242, https://doi.org/10.1016/j.matdes.2023.112242.
[7] Y. Yan, W.-G. Kim, X. Ma, T. Tegafaw, T.M. Nguyen, J.-M. Lee, E.-J. Choi, H. Ahn, S.-H. Ha, K. Kim, J.-M. Kim, H.K. Kim, J.-W. Oh, D.-M. Shin, Y.-H. Hwang, Nanogenerators facilitated piezoelectric and flexoelectric characterizations for bioinspired energy harvesting materials, Nano Energy 81 (2021) 105607, https://doi.org/10.1016/j.nanoen.2020.105607.
[8] M.-C. Huang, C.-H. Xue, Z. Bai, J. Cheng, Y.-G. Wu, C.-Q. Ma, L. Wan, L. Xie, H.-D. Wang, B.-Y. Liu, X.-J. Guo, Bioinspired smart dual-layer hydrogels system with synchronous solar and thermal radiation modulation for energy-saving all-season temperature regulation, J. Energy Chem. 101 (2025) 175–190, https://doi.org/10.1016/j.jechem.2024.09.051.
[9] X. Wu, J. Deng, W. Jian, Y. Yang, H. Shao, X. Zhou, Y. Xiao, J. Ma, Y. Zhou, R. Wang, H. Li, A bioinspired switchable adhesive patch with adhesion and suction mechanisms for laparoscopic surgeries, Mater. Today Bio 27 (2024) 101142, https://doi.org/10.1016/j.mtbio.2024.101142.
[10] A.S. Raikar, D.M. Kalaskar, S. Bhilegaonkar, S.N. Somnache, M. Bodaghi, Revolutionizing drug delivery by bioinspired 4D transdermal microneedles: advances and future horizons, Eur. Polym. J. 210 (2024) 112952, https://doi.org/10.1016/j.eurpolymj.2024.112952.
[11] P.W. Sayyad, S.-J. Park, T.-J. Ha, Bioinspired nanoplatforms for human-machine interfaces: recent progress in materials and device applications, Biotechnol. Adv. 70 (2024) 108297, https://doi.org/10.1016/j.biotechadv.2023.108297.
[12] X. Lu, S. Zhao, W. Chen, H. Xie, J. Teng, L. Ren, K. Wang, Z. Qian, L. Ren, Bioinspired multilayer braided structure with controllable nonlinear mechanical properties for artificial ligaments, Mater. Des. 241 (2024) 112976, https://doi.org/10.1016/j.matdes.2024.112976.
[13] M. Chen, Q. Wang, M. Trubyanov, K. Yang, A.S. Aglikov, G. Qi, E.V. Skorb, K. S. Novoselov, D.V. Andreeva, Large-scale self-assembly of anisotropic graphene oxide films via blade coating: sustainable design and Stimuli-Responsive performance for biomimicry, Mater. Des. 233 (2023) 112205, https://doi.org/10.1016/j.matdes.2023.112205.
[14] A. Sensini, R. D'Anniballe, C. Gotti, G. Marchiori, G. Giavaresi, R. Carloni, M. Letizia Focarete, A. Zucchelli, Bi-material nanofibrous electrospun junctions: a versatile tool to mimic the muscle–tendon interface, Mater. Des. 242 (2024) 113015, https://doi.org/10.1016/j.matdes.2024.113015.
[15] S. Hu, C. Li, H. Wang, M.D. Mylo, J. Becker, B. Cao, C. Müller, C. Eberl, K. Yin, Swelling and deswelling driven multimaterials silicone hopper with superior specific power and energy, Mater. Des. 241 (2024) 112960, https://doi.org/10.1016/j.matdes.2024.112960.
[16] U.G.K. Wegst, M.F. Ashby, The mechanical efficiency of natural materials, Philos. Mag. 84 (2004) 2167–2186, https://doi.org/10.1080/14786430410001680935.
[17] F. Barthelat, H. Tang, P. Zavattieri, C. Li, H. Espinosa, On the mechanics of mother-of-pearl: a key feature in the material hierarchical structure, J. Mech. Phys. Solids 55 (2007) 306–337, https://doi.org/10.1016/j.jmps.2006.07.007.
[18] S. Alvarez, P. Marcasuzaa, L. Billon, Bio-inspired silica films combining block copolymers self-assembly and soft chemistry: paving the way toward artificial exosqueleton of seawater diatoms, Macromol. Rapid Commun. 42 (2021) 2000582, https://doi.org/10.1002/marc.202000582.
[19] T. Coradin, P.J. Lopez, C. Gautier, J. Livage, From biogenic to biomimetic silica, C. R. Palevol 3 (2004) 443–452, https://doi.org/10.1016/j.crpv.2004.07.002.
[20] C. Lechner, C. Becker, Silaffins in silica biomineralization and biomimetic silica precipitation, Mar. Drugs 13 (2015) 5297–5333, https://doi.org/10.3390/md13085297.
[21] N. Nassif, J. Livage, From diatoms to silica-based biohybrids, Chem. Soc. Rev. 40 (2011) 849–859, https://doi.org/10.1039/C0CS00122H.
[22] J. Aizenberg, J. Livage, S. Mann, New developments in bio-related materials, J. Mater. Chem. 14 (2004) E5, https://doi.org/10.1039/b409121n.
[23] W. Hu, Z. Zheng, J. Jiang, Vertical organic-inorganic hybrid transparent oxide TFTs gated by biodegradable electric-double-layer biopolymer, Org. Electron. 44 (2017) 1–5, https://doi.org/10.1016/j.orgel.2017.02.001.
[24] Y. Wang, Z. Liu, H. Pan, R. Tang, Biomineralization inspired crystal growth for biomimetic materials preparation, J. Cryst. Growth 603 (2023) 127029, https://doi.org/10.1016/j.jcrysgro.2022.127029.
[25] L.R. Oliveira, E.J. Nassar, H. Da Silva Barud, J.M. Silva, L.A. Rocha, Polymer and biopolymer organic-inorganic composites containing mixed oxides for application in energy up- and down-conversion, Opt. Mater. 134 (2022) 113189, https://doi.org/10.1016/j.optmat.2022.113189.
[26] P. Pal, A. Pal, K. Nakashima, B.K. Yadav, Applications of chitosan in environmental remediation: a review, Chemosphere 266 (2021) 128934, https://doi.org/10.1016/j.chemosphere.2020.128934.
[27] J. Retuert, R. Quijada, V. Arias, M. Yazdani-Pedram, Porous silica derived from chitosan-containing hybrid composites, J. Mater. Res. 18 (2003) 487–494, https://doi.org/10.1557/JMR.2003.0062.
[28] M. Kalaiyarasan, S. Pugalmani, N. Rajendran, Fabrication of chitosan/silica hybrid coating on AZ31 Mg alloy for orthopaedic applications, J. Magnes. Alloys 11 (2023) 614–628, https://doi.org/10.1016/j.jma.2022.05.003.
[29] S. Zhang, Y. Liao, K. Lu, Z. Wang, J. Wang, L. Lai, W. Xin, Y. Xiao, S. Xiong, F. Ding, Chitosan/silica hybrid aerogels with synergistic capability for superior hydrophobicity and mechanical robustness, Carbohydr. Polym. 320 (2023) 121245, https://doi.org/10.1016/j.carbpol.2023.121245.
[30] M. Lazari, F. Elmi, Structural study of coated wood with superhydrophobic chitosan/silica hybrid nanocomposite in seawater, Prog. Org. Coat. 186 (2024) 108076, https://doi.org/10.1016/j.porgcoat.2023.108076.
[31] T. Suzuki, Y. Mizushima, Characteristics of silica-chitosan complex membrane and their relationships to the characteristics of growth and adhesiveness of L-929 cells cultured on the biomembrane, J. Ferment. Bioeng. 84 (1997) 128–132, https://doi.org/10.1016/S0922-338X(97)82541-X.
[32] F. Al-Sagheer, S. Muslim, Thermal and mechanical properties of chitosan/SiO_2 hybrid composites, J. Nanomater. 2010 (2010) 490679, https://doi.org/10.1155/2010/490679.
[33] S.-M. Lai, A.-J.-M. Yang, W.-C. Chen, J.-F. Hsiao, The properties and preparation of chitosan/silica hybrids using sol-gel process, Polym.-Plast. Technol. Eng. 45 (2006) 997–1003, https://doi.org/10.1080/03602550600726269.
[34] N.H. Ibrahim, A. Iqbal, N. Mohammad-Noor, M.R. Roziawati, S. Sreekantan, A. S. Zulkipli, Feasibility of chitosan thin film and hybrid chitosan/silica thin film for the mitigation of toxic Alexandrium minutum, Mater. Today Proc. 57 (2022) 1184–1190, https://doi.org/10.1016/j.matpr.2021.10.192.
[35] A. Larrieu, P. Marcasuzaa, C. Courreges, L. Billon, Biohybrid chitosan/silica self-supported films by soft chemistry in aqueous media: Biomimetic mineralization of Diatoms exoskeleton, Surf. Interf. 51 (2024) 104675, https://doi.org/10.1016/j.surfin.2024.104675.
[36] J. Geltmeyer, G. Vancoillie, I. Steyaert, B. Breyne, G. Cousins, K. Lava, R. Hoogenboom, K. De Buysser, K. De Clerck, Dye modification of nanofibrous silicon oxide membranes for colorimetric HCl and NH_3 sensing, Adv. Funct. Mater. 26 (2016) 5987–5996, https://doi.org/10.1002/adfm.201602351.
[37] I. Sousa, M.C. Quevedo, A. Sushkova, M.G.S. Ferreira, J. Tedim, Chitosan microspheres as carriers for pH-indicating species in corrosion sensing, Macromol. Mater. Eng. 305 (2020) 1900662, https://doi.org/10.1002/mame.201900662.
[38] A. Dirpan, R. Latief, A. Syarifuddin, A.N.F. Rahman, R.P. Putra, S.H. Hidayat, The use of colour indicator as a smart packaging system for evaluating mangoes Arummanis (*Mangifera indica* L. var. Arummanisa) freshness, IOP Conf. Ser. Earth Environ. Sci. 157 (2018) 012031, https://doi.org/10.1088/1755-1315/157/1/012031.
[39] Y.S. Musso, P.R. Salgado, A.N. Mauri, Gelatin based films capable of modifying its color against environmental pH changes, Food Hydrocoll. 61 (2016) 523–530, https://doi.org/10.1016/j.foodhyd.2016.06.013.
[40] I.M. El-Nahhal, S.M. Zourab, F.S. Kodeh, F.H. Abdelsalam, Sol–gel encapsulation of bromothymol blue pH indicator in presence of Gemini 12-2-12 surfactant, J. Sol-Gel Sci. Technol. 71 (2014) 16–23, https://doi.org/10.1007/s10971-014-3324-6.
[41] H.M.F.A. El-Wahab, G.-S.-E.-D. Moram, Toxic effects of some synthetic food colorants and/or flavor additives on male rats, Toxicol. Ind. Health 29 (2013) 224–232, https://doi.org/10.1177/0748233711433935.
[42] T. Taguchi, Y. Kohno, M. Shibata, Y. Tomita, C. Fukuhara, Y. Maeda, An easy and effective method for the intercalation of hydrophobic natural dye into organo-montmorillonite for improved photostability, J. Phys. Chem. Solids 116 (2018) 168–173, https://doi.org/10.1016/j.jpcs.2018.01.027.
[43] P. Trigueiro, F.A.R. Pereira, D. Guillermin, B. Rigaud, S. Balme, J.-M. Janot, I.M. G. dos Santos, M.G. Fonseca, P. Walter, M. Jaber, When anthraquinone dyes meet pillared montmorillonite: Stability or fading upon exposure to light, Dyes Pigments 159 (2018) 384–394, https://doi.org/10.1016/j.dyepig.2018.06.046.
[44] M. Ogawa, R. Takee, Y. Okabe, Y. Seki, Bio-geo hybrid pigment; clay-anthocyanin complex which changes color depending on the atmosphere, Dyes Pigments 139 (2017) 561–565, https://doi.org/10.1016/j.dyepig.2016.12.054.
[45] A. Claro, M.J. Melo, S. Schäfer, J.S.S. de Melo, F. Pina, K.J. van den Berg, A. Burnstock, The use of microspectrofluorimetry for the characterization of lake pigments, Talanta 74 (2008) 922–929, https://doi.org/10.1016/j.talanta.2007.07.036.
[46] R. Sánchez-de-Armas, J. Oviedo López, M.A. San-Miguel, J. Fdez, P. Sanz, M. P. Ordejón, Real-time TD-DFT simulations in dye sensitized solar cells: the electronic absorption spectrum of alizarin supported on TiO_2 nanoclusters, J. Chem. Theory Comput. 6 (2010) 2856–2865, https://doi.org/10.1021/ct100289t.
[47] D. Verma, K.S. Katti, D.R. Katti, Osteoblast adhesion, proliferation and growth on polyelectrolyte complex–hydroxyapatite nanocomposites, Philos. Trans. R. Soc. Math. Phys Eng. Sci. 368 (2010) 2083–2097, https://doi.org/10.1098/rsta.2010.0013.
[48] P. Ezati, H. Tajik, M. Moradi, Fabrication and characterization of alizarin colorimetric indicator based on cellulose-chitosan to monitor the freshness of minced beef, Sens. Actuators B Chem. 285 (2019) 519–528, https://doi.org/10.1016/j.snb.2019.01.089.
[49] Y. Kumar, Y. Bist, D. Thakur, M. Nagar, D.C. Saxena, A review on the role of pH-sensitive natural pigments in biopolymers based intelligent food packaging films, Int. J. Biol. Macromol. 276 (2024) 133869, https://doi.org/10.1016/j.ijbiomac.2024.133869.
[50] S.-H. Jun, E.-J. Lee, S.-W. Yook, H.-E. Kim, H.-W. Kim, Y.-H. Koh, A bioactive coating of a silica xerogel/chitosan hybrid on titanium by a room temperature

sol–gel process, Acta Biomater. 6 (2010) 302–307, https://doi.org/10.1016/j.actbio.2009.06.024.
[51] B. Palla-Rubio, N. Araújo-Gomes, M. Fernández-Gutiérrez, L. Rojo, J. Suay, M. Gurruchaga, I. Goñi, Synthesis and characterization of silica-chitosan hybrid materials as antibacterial coatings for titanium implants, Carbohydr. Polym. 203 (2019) 331–341, https://doi.org/10.1016/j.carbpol.2018.09.064.
[52] M. Spontón, D. Estenoz, G. Lligadas, J.C. Ronda, M. Galià, V. Cádiz, Synthesis and characterization of a hybrid material based on a trimethoxysilane functionalized benzoxazine, J. Appl. Polym. Sci. 126 (2012) 1369–1376, https://doi.org/10.1002/app.36766.
[53] I. Bravo-Flores, M. Meléndez-Zamudio, A. Guerra-Contreras, E. Ramírez-Oliva, G. Álvarez-Guzmán, R. Zárraga-Núñez, A. Villegas, J. Cervantes, Revisiting the System Silanes–Polysaccharides: The Cases of THEOS–Chitosan and MeTHEOS–Chitosan, Macromol. Rapid Commun. 42 (2021) 2000612, https://doi.org/10.1002/marc.202000612.
[54] Z. Liu, W. Shi, Y. Lei, Z. Xie, Novel polyamide/silica/chitosan covalent hybrid: One-step BIC/sol-gel preparation at room temperature and dual applications in Hg^{2+} electrochemical probing and dye adsorption, Carbohydr. Polym. 312 (2023) 120808, https://doi.org/10.1016/j.carbpol.2023.120808.
[55] T. Ohishi, Y. Yamazaki, T. Nabatame, Preparation, structure and gas barrier characteristics of poly silazane-derived silica thin film formed on PET by simultaneously applying ultraviolet-irradiation and heat-treatment, Front. Nanosci. Nanotechnol. 2 (2016), https://doi.org/10.15761/FNN.1000126.
[56] C. Pandis, S. Madeira, J. Matos, A. Kyritsis, J.F. Mano, J.L.G. Ribelles, Chitosan–silica hybrid porous membranes, Mater. Sci. Eng. C 42 (2014) 553–561, https://doi.org/10.1016/j.msec.2014.05.073.
[57] Z. Yu, B. Li, J. Chu, P. Zhang, Silica in situ enhanced PVA/chitosan biodegradable films for food packages, Carbohydr. Polym. 184 (2018) 214–220, https://doi.org/10.1016/j.carbpol.2017.12.043.
[58] B.P. Tripathi, V.K. Shahi, Functionalized organic-inorganic nanostructured N-p-carboxy benzyl chitosan-silica-PVA hybrid polyelectrolyte complex as proton exchange membrane for DMFC applications, J. Phys. Chem. B 112 (2008) 15678–15690, https://doi.org/10.1021/jp806337b.
[59] L. Cui, J. Jia, Y. Guo, Y. Liu, P. Zhu, Preparation and characterization of IPN hydrogels composed of chitosan and gelatin cross-linked by genipin, Carbohydr. Polym. 99 (2014) 31–38, https://doi.org/10.1016/j.carbpol.2013.08.048.
[60] Y. Liu, Z. Cai, L. Sheng, M. Ma, Q. Xu, Influence of nanosilica on inner structure and performance of chitosan-based films, Carbohydr. Polym. 212 (2019) 421–429, https://doi.org/10.1016/j.carbpol.2019.02.079.
[61] L. Ghannam, H. Garay, M.E.R. Shanahan, J. François, L. Billon, A new pigment type: colored diblock copolymer−mica composites, Chem. Mater. 17 (2005) 3837–3843, https://doi.org/10.1021/cm0478024.
[62] L. Ghannam, H. Garay, L. Billon, Sensitive colored hybrid inorganic/organic pigments based on polymer-coated microsized particles, Macromolecules 41 (2008) 7374–7382, https://doi.org/10.1021/ma800522k.
[63] M. Joubert, A. Khoukh, J.-F. Tranchant, F. Morvan, L. Billon, Hybrid aluminum colored pigments based on gradient copolymers design, Macromol. Chem. Phys. 210 (2009) 1544–1555, https://doi.org/10.1002/macp.200900254.